Mem. Fac. Sci. Kyoto Univ. (Ser. Biol.), 18: 109-118, Dec., 2006

Quantitative Analysis of Hominoid Upper Molar Shape: Visualization of Ridges, Valleys and Curvature

MASAYO ABE

Laboratory of Physical Anthropology, Department of Zoology, Kyoto University, Sakyo, Kyoto, 606-8502 Japan
(Received November 27, 2006)

Abstract The three-dimensional morphology of the tooth is closely related to the dietary habits of primates. However, quantitative treatment of tooth morphology depends largely on linear, angular, and/or area measurements. Crown surface topology, such as curvature, has rarely been analyzed quantitatively. In the present study, an algorithm for evaluating regional or global convexity and for detecting ridge and valley lines in the occlusal surface of hominoid molars is proposed. A computer reconstructed crown surface is treated as a two-dimensional function on a grid system. The regional curvature is approximated with a quadratic surface using the Taylor expansion. The convexity at the point can be estimated using the mean curvature, which is defined by the summation of two principle curvatures of the quadratic surface. Ridge and valley lines are considered as sets of points at which the vertex of the parabola extracted from the quadratic curve along the first principle direction is sufficiently close to the point. As the differential operators for the curvature calculation, the derivative of the two-dimensional Gaussian function is employed. By changing the parameter of the Gaussian function, structures from regional to global can be depicted separately. The proposed method is applied to first upper molars of hominoids, and the usefulness of the proposed method is verified.

Key words Molar shape, Image processing, Ridge and valley detection, Curvature

Introduction

Tooth morphology in living primates varies depending on dietary habits. For careful analysis of this relationship, the quantitative treatment of shape and size of teeth is the principal requisite (Goto & Ohtaishi 1986; Colbert & Morales 1991; Fleagle 1999). Numerous studies have been published for tooth shape variation in primates (Compton & Sita-Lumsden 1970; Wood 1983; Matsumura 1992; Ishida *et al.* 1994, 1995). In most of these studies, tooth shape was analyzed by ratios of linear measurements, angles defined by landmarks, or the relative area of the reflected crown surface (Kay 1974, 1975, 1977; Wood & Abbott 1983; Wood & Engelman 1988; Hartman 1989). The recent development of measurement devices, such as the micro CT or the laser surface scanner, has enabled researchers to obtain fine-scale three-dimensional morphological data of the tooth. Coupled with the dramatic increase in the processing ability of personal computers, various visualization methods have recently been proposed (Kono-Takeuchi 1998; Spoor *et al.* 1993).

A number of researchers have analyzed the laser-scanned crown surface by using the Geographic Resources Analysis Support System (GRASS) (Zuccotti *et al.* 1998; Ungar &

Williamson 2000; Ungar 2004). While this method is effective for visualizing the crown surface morphology and for calculating the surface area or angulation, users cannot extract variously defined measurements because the software is developed for geographic analysis so that functions useful for molar shape analysis are limited. In the present study, an algorithm for evaluating surface topographic features, such as the convexity of surface or ridge/valley patterns, is proposed, and application of the proposed algorithm to hominoid molars is demonstrated.

Materials and Methods

Materials

In the present study, the first upper molars of the orangutan (*Pongo pygmaeus*), the gorilla (*Gorilla gorilla*), the bonobo (*Pan paniscus*), and the chimpanzee (*Pan troglodytes*) were treated. The upper molar has four main cusps, arranged in a trigon and a hypocone. The trigon has three cusps arranged in a triangle.

The surface shapes of several molars were measured using a 3D-scanner PICZA PIX-4 (Roland-DG, Japan) that provides three-dimensional positions of sample points on the surface. A tooth is fixed on the xy-stage of the scanner with clay and is moved in the x- and y-directions with a constant pitch in a specified rectangular region. After each movement, a needle of the scanner descends vertically until its tip touches the tooth surface, and the height (z-value) of the tip is then measured at the position (x, y). As a result, a height list at regular intervals can be obtained. Since the x- and y-pitches are identical and constant, the surface shape is represented by a two-dimensional image in which each pixel value is the height of the surface. These images are examined in the present study.

Method

The curved surface of a tooth is represented by a two-dimensional function $z = f(x,y)$ where (x,y,z) is the three-dimensional position of a measured point. According to the Taylor expression, the surface around a measured point can be approximated as

$$f(x+dx,y+dy) \cong f(x,y) + \nabla f(x,y)\begin{pmatrix} dx \\ dy \end{pmatrix} + \frac{1}{2}(dx,dy)\mathbf{H}(x,y)\begin{pmatrix} dx \\ dy \end{pmatrix} \quad (1)$$

$\nabla f(x,y)$ is the gradient of $f(x,y)$ at each measured point and is given as

$$\nabla f(x,y) \equiv \left(\frac{\partial f}{\partial x}, \frac{\partial f}{\partial y}\right) \quad (2)$$

$\mathbf{H}(x,y)$ is the Hesse matrix, which is defined as

$$\mathbf{H}(x,y) \equiv \begin{pmatrix} \dfrac{\partial^2 f}{\partial x^2} & \dfrac{\partial^2 f}{\partial x \partial y} \\ \dfrac{\partial^2 f}{\partial x \partial y} & \dfrac{\partial^2 f}{\partial y^2} \end{pmatrix} \tag{3}$$

Since $f(x,y)$ is discrete, the differential functions shown in Eqs. 2 and 3 cannot be calculated as a continuous function. Therefore, an approximation method based on Gaussian smoothing is proposed as described later herein.

When the i-th eigenvalue and the corresponding i-th eigenvector of $\mathbf{H}(x,y)$ are given as λ_i and $\boldsymbol{v}_i$ $(i=1,2;\ |\boldsymbol{v}_i|=1)$, respectively, $\nabla f(x,y)$ and (dx,dy) can be written as follows:

$$\begin{aligned} \nabla f(x,y) &= \sum_{i=1}^{2} \alpha_i \boldsymbol{v}_i \\ (dx,dy) &= \sum_{i=1}^{2} \xi_i \boldsymbol{v}_i \end{aligned} \tag{4}$$

where α_i $(i=1,2)$ and ξ_i $(i=1,2)$ are coefficients, and the subscript "i" denotes the number of eigenmodes of $\mathbf{H}(x,y)$. Since $\mathbf{H}(x,y)$ is a symmetric matrix, $\boldsymbol{v}_i \cdot \boldsymbol{v}_j = 0\,(i \neq j)$, Eq. 1 can be rewritten as

$$\begin{aligned} f(x+dx,y+dy) &\cong f(x,y) + \sum_{i=1}^{2} \alpha_i \xi_i + \frac{1}{2}\sum_{i=1}^{2} \lambda_i \xi_i^2 \\ &= \frac{1}{2}\sum_{i=1}^{2} \lambda_i \left(\xi_i + \frac{\alpha_i}{\lambda_i}\right)^2 + f(x,y) - \frac{1}{2}\sum_{i=1}^{2} \frac{\alpha_i^2}{\lambda_i} \\ &\equiv C(\xi_1,\xi_2) \end{aligned} \tag{5}$$

Equation 5 indicates that the curved shape around any measured point can be approximated by a quadratic curved surface $C(\xi_1,\xi_2)$.

The definition of curvature on the curved surface depends on the choice of a curved line on the surface. As such, there are various definitions of curvature. In addition, for a complex tooth shape, as yet no method has been proposed for evaluating the curvature. Thus, in the present study, a new and simple method of curvature estimation for teeth surfaces is presented. In particular, the proposed method for selecting ridge and valley points provides a novel image processing method.

Two curved lines are decided by substituting ξ_2 or ξ_1 to 0 in Eq. 5, i.e., $C(\xi_1,0)$ and $C(0,\xi_2)$. These two parabolic curves, simply expressed by $C_1(\xi)$ and $C_2(\xi)$, are the intersections of the curved surface and the plane, which is orthogonal to ν_i $(i=1,2)$. The two curved lines $C_i(\xi)$ are then written as

$$C_i(\xi)=\frac{1}{2}\lambda_i\left(\xi+\frac{\alpha_i}{\lambda_i}\right)^2+f(x,y)-\frac{1}{2}\frac{\alpha_i^2}{\lambda_i} \qquad (i=1,2) \tag{6}$$

The curvature $\kappa_i(\xi)$ at the point ξ of $C_1(\xi)$ is given as

$$\kappa_i(\xi)=\frac{\dfrac{\partial^2 C_i}{\partial\xi^2}}{\left[1+\left\{\dfrac{\partial C_i}{\partial\xi}\right\}^2\right]^{\frac{3}{2}}} \qquad (i=1,2) \tag{7}$$

and so $\kappa_i(\xi)$ at the measured point $\xi=0$, $\kappa_i(0)$ which is simply symbolized with κ_i hereinafter, is calculated by the following equation using Eqs. 6 and 7:

$$\kappa_i=\frac{\lambda_i}{(1+\alpha_i^2)^{\frac{3}{2}}} \qquad (i=1,2) \tag{8}$$

In particular, in Eq. 8, the sign of $\kappa_i(0)$ or λ_i denotes the convexity $(\kappa_i<0)$, the concavity $(\kappa_i>0)$ or the flatness $(\kappa_i=0)$ of the curve, and the sign of the mean curvature $\overline{\kappa}$, defined by $\overline{\kappa}\equiv(\kappa_1+\kappa_2)/2$, indicates the mean convexity.

At ridge or valley points, the absolute value of one of the two curvatures is much larger than the other. These points are very near the vertex of the parabola, which gives the larger curvature. After this, $|\kappa_1|$ is assumed to be greater than or equal to $|\kappa_2|$. Since the distance from the measured point to the vertex is given by $|\alpha_1/\lambda_1|$, a measured point is regarded as a ridge or valley point if $|\alpha_1/\lambda_1|$ is less than 1.0 pitch of the measured points.

Although the following processing method on differential operation is common in the signal processing field, a rough outline is provided because the proposed method is used to extract the regional or global shape of tooth. In general, differential operation enhances the noise added to a true value because each noise value is different among adjacent points, which is in contrast to the slow change of the true value, and the differential operator tends to enlarge the former fast change. Therefore, differential calculation is generally combined with a smoothing operation. However, there are various types of smoothing operators. Moreover, smoothing effects differ depending on the operators and their parameters. In the present study, a Gaussian smoothing filter, $F_{gauss}(x,y)$, defined as follows:

$$F_{gauss}(x,y) = \frac{1}{2\pi\sigma^2}\exp\left\{-\frac{(x^2+y^2)}{2\sigma^2}\right\} \tag{9}$$

is employed because of the ease with which the results can be controlled.

In Eq. 9, σ is a parameter of $F_{gauss}(x,y)$, which controls its smoothing effect. The smoothed function, $\tilde{f}(x,y)$, is calculated using a convolution operator $\otimes$, as follows:

$$\begin{aligned}\tilde{f}(x,y) &= f(x,y)\otimes F_{gauss}(x,y)\\ &= \sum_X\sum_Y f(X,Y)\cdot F_{gauss}(x-X,y-Y)\end{aligned} \tag{10}$$

Equation 10 indicates that $\tilde{f}(x,y)$ is a weighted average of $f(x,y)$ and the smoothing effect increases as σ increases. Considering the complex shape of the tooth, small σ refers to the detailed shape, whereas large σ refers to the global shape.

Then, the differential operation to $\tilde{f}(x,y)$ is given as

$$\begin{aligned}\partial\tilde{f}(x,y)/\partial x &= \tilde{f}(x,y)\otimes\frac{\partial}{\partial x}\\ &= f(x,y)\otimes F_{gauss}(x,y)\otimes\frac{\partial}{\partial x}\\ &= f(x,y)\otimes\frac{\partial F_{gauss}(x,y)}{\partial x}\end{aligned} \tag{11}$$

Equation 11 indicates that the combination of smoothing and differential operators to $f(x,y)$ is given by the first derivative of the smoothing operator. Similarly, the second derivative of $F_{gauss}(x,y)$ gives the combination of smoothing and the second-order differential operator. Signal processing and image processing are described in greater detail in a number of sources (Taubin 1995; Malladi & Ethian 1996; Desbrun 1999; Kobbelt 2000; Ohtake 2000).

The algorithm described above was implemented on a PowerBook G3 (Apple Computer Inc., USA).

Results

Figure 1 shows an example of the processing result of a first molar of Pan paniscus. Minor differences between Figs. 1b and 1c show that smoothing with a σ of 1 pixel has a very small effect. On the other hand, smoothed contour lines in Fig. 1d and blurred contrast in Fig. 1f denotes that a σ of 5 pixels is sufficiently large to eliminate the

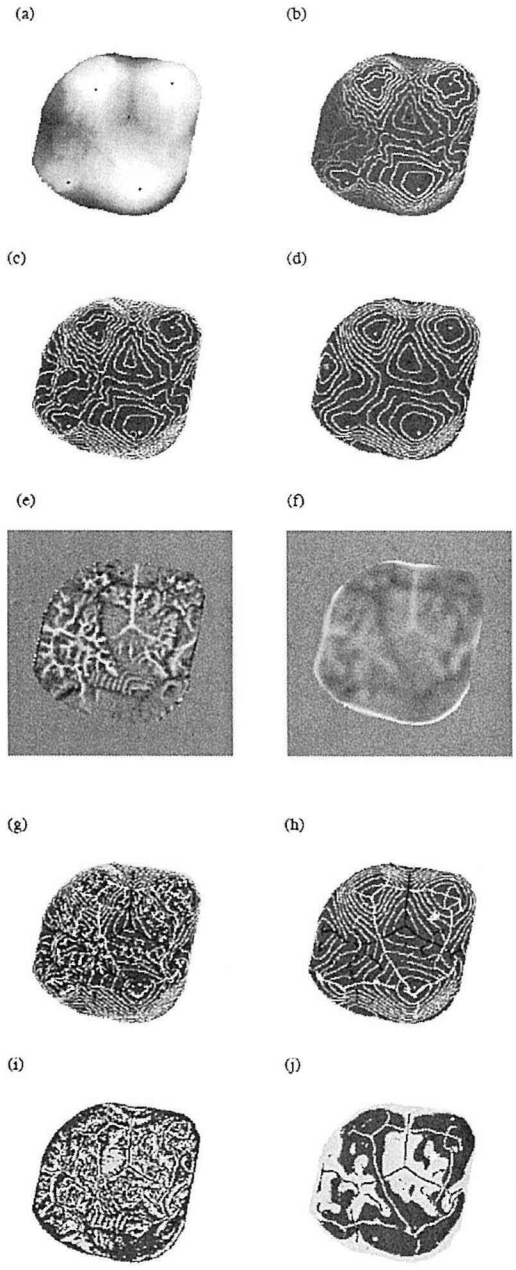

Fig. 1. Examples of results. The parameter σ for the calculations in (c), (e), (g) and (i) is 1, and that for the calculations in (d), (f), (h) and (j) is 5. (a) Original image of tooth shape (*Pan paniscus*). The black points denote the peaks of the cusps and the base of the trigon basin. (b) Contour image of (a). (c), (d) Contour images after smoothing. (e), (f) Mean curvature images after smoothing. White and black colors indicate concavity and convexity, respectively. (g), (h) Complex visualization of the detected ridges (white) and valleys (black) superimposed on contour images. (i), (j) Detected ridges and valleys superimposed on the convexity maps derived by thresholding the corresponding contour images with the threshold value of 0. Light and dark gray areas denote concavity and convexity, respectively.

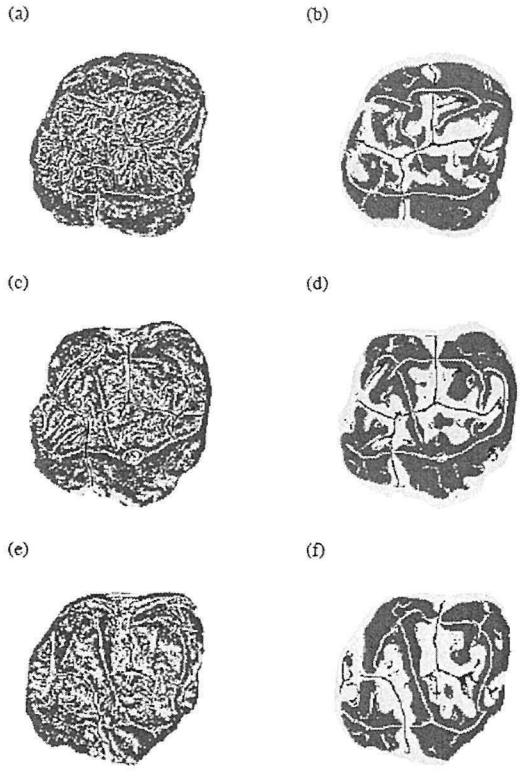

Fig. 2. Differences in surface shape among *Pongo pygmaeus* (a, b), *Gorilla gorilla* (c, d) and *Pan troglodytes* (e, f) visualized in the same manner as Figs. 1i and 1j. The parameter σ for the calculations for the images of the left and right columns are 1 and 5, respectively.

regional shape without changing its global shape. In Fig. 1e, minute convex or concave shapes of wrinkles on the surface can be visualized, whereas these wrinkles are not observed in Figs. 1a and 1b. Although ridge and valley points are detected one by one, they appear as continuous lines in Figs. 1h and 1j. This means that ridge and valley lines are detected correctly. Figures 1i and 1j show that complex ridge and valley patterns are observed on the image with small σ, but that smoothed and global patterns are detected with large σ. This indicates that the smoothing effect mentioned above works effectively. With the convexity map shown in Figs. 1i and 1j, convex and concave shapes can be distinguished immediately. Especially in areas where the absolute values of the curvature are small compared with the ridge and valley areas, the convexity map is useful because the distinction is difficult with the curvature image.

Figure 2 shows the differences in surface shapes among *Pongo pygmaeus*, *Gorilla gorilla* and *Pan troglodytes*. In all cases, ridge and valley lines are detected clearly. In the images with smaller σ (left column), regional shapes are depicted well. In particular, wrinkles that are indicated by line patterns of ridge (white) and valley (black) lines are

observed in Figs. 2a and 2c. In contrast, compared with the other images, in Fig. 2e, the valley lines in the trigon region are not clear. In the images with larger σ (right column), the trigon region surrounded by ridge lines can be depicted roughly. Even in the image of *Pongo pygmaeus* in Fig. 2b, the trigon region is clearly observed, whereas this is not the case in Fig. 2a. These images show that, in any species, the trigon is composed of three ridge lines that connect three main cusps and three valley lines that diverge from the base of the trigon basin to the midpoints of the ridge lines. Despite having the name "trigon", the shape of the trigon region is a quadrilateral rather than triangular because the buccal-lingual ridge lines are connected not to the peak of the protocone, but to the mesial-distal ridge line that passes across the peak. In particular, in *Pongo pygmaeus* and *Gorilla gorilla*, the buccal-lingual spans between the two mesial-distal ridge lines are narrow, so that the shape of the trigon region is nearly square.

Discussion

The present algorithm enables detection of the ridge and valley lines on the curved surface of the molar and quantification of the convexity of the surface by calculating curvatures. In addition, using this method, regional and global features are evaluated separately by controlling the parameter σ of the smoothing operator in Eq. 9. Considering that the outer edge of the trigon of the first molar is defined by ridge lines, the ridge lines detected with large σ allows us to obtain the trigon shape automatically. The complexity of the ridge and valley pattern detected with small σ might be useful for explaining the relationship between masticating behavior and tooth shape (occlusal surface).

The inter-species shape difference of the molars of different species (Figs. 1 & 2) revealed herein may explain the relationship between the occlusal surface and dietary habits. The molars of *Pongo pygmaeus*, which have distinct wrinkles, are thought to be useful for crushing and grinding seeds. The large trigon region and fewer wrinkles in *Pan paniscus* (Fig.1i) and *Pan troglodytes* (Fig. 2e) may be related to the fact that fruit-eaters need a large occlusal area, rather than wrinkles for crushing softer food. In contrast, relatively a small trigon region and smaller wrinkles in *Pongo pygmaeus* and *Gorilla gorilla* might indicate that forces needed for crushing seeds or leaves are concentrated in the trigon region (Fleagle 1999). Thus, wrinkles and the shape of trigon region can be informative in the investigation of dietary habits. The proposed method may provide details of wrinkles, e.g., their depth or width, with changing σ. With this advantage, it may be possible to advance the study of the relationship between occlusal surface and masticating function (Compton & Sita-Lumsden 1970; Kay 1975, 1977; Wood 1983; Matsumura *et al.*1992; Ishida *et al.* 1994, 1995; Fleagle 1999).

There are two reasons for dealing with two-dimensional images, although the shape of the tooth is three-dimensional. One reason is that, as a subject, only the upper molar surface, which can be expressed with a single valued function, is selected. The other reason is that two-dimensional image processing is easier and faster than three-dimensional image processing. However, for two-dimensional images, the results depend on the

positioning of the tooth in measuring the surface. Strictly speaking, the position of the tooth is thought to be oriented by the cervical line, but cervical lines are difficult to decide correctly. Therefore, other standards for orienting the sample are needed in order to compare the results of feature detection among different teeth.

On the other hand, recent studies of micro X-ray CT have demonstrated the feasibility of three-dimensional shape acquisition and visualization of a tooth. The proposed method can be expanded to three-dimensions. First, the curved surface is extracted from the volume data by thresholding. Then, a new Cartesian coordinate should be re-defined at each measured point, for example, using the tangent space or principal component analysis. Finally, the proposed method is applied to measured points around the target point on the new coordinate system.

Acknowledgments

The author would like to thank Professor Hidemi Ishida of University of Shiga Prefecture for his helpful advice and encouragement. The author is also grateful to Associate Professor Masato Nakatuskasa and Assistant Professor Naomichi Ogihara of Kyoto University for a critical reading of the manuscript. This study was partly supported by the 21st COE Program (A14).

References

Colbert, E. H. & M. Morales 1991 Evolution of the vertebrates. (4th ed.), Wiley-Liss, Inc., New York.

Compton, A. W. & A. Sita-Lumsden 1970 Functional significance of the therian molar pattern. Nature 227: 197-199.

Desbrun, M., M. Meyer, P. Schroder & A. Barr 1999 Implicit fairing of irregular meshes using diffusion and curvature flow. Siggraph '99.

Fleagle, J. G. 1999 Primate adaptation and evolution. (2nd ed.). Academic Press, San Diego.

Goto, M. & N. Ohtaishi 1986 Comparative ontology-morphology, function and evolution of tooth in vertebrates. Ishiyaku Publishers, Inc., Tokyo. (in Japanese)

Hartman, S. E. 1989 Stereophotogrammetric analysis of occlusal morphology of extant hominoid molars: phenetics and function. Am. J. Phys. Anthropol. 80: 145-166.

Ishida, H., M. Nakatsukasa, M. Yamashita & Y. Kunimatsu 1994 Three dimensional analysis of the trigon basins of the first upper molars in gorillas and Kenyapithecus from Nachola, a preliminary study. Anthrop. Sci. 102: 178.

Ishida, H., D. Shimizu & Y. Kunimatsu 1995 A three dimensional analysis of morphology of the upper 1st molars of orangutans. Primate Res. 11: 307.

Kay, R. F. 1974 Jaw movement and tooth use in recent and fossil primates. Am. J. Phys. Anthropol. 40: 227-256.

Kay, R. F. 1975 The functional adaptations of primate molar teeth. Am. J. Phys. Anthropol. 43: 195-216.

Kay, R. F. 1977 The evaluation of molar occlusion in the Cercopithecidae and early catarrhines. Am. J. Phys. Anthropol. 46: 327-352.

Kobbelt, L. 2000 Discrete fairing and variational subdivision for freeform surface design. The Visual Comput. 16: 142-158.

Kono-Takeuchi, R., G. Sura, E. Kanazawa & T. Tanijiri 1998 A new method of evaluating enamel thickness based on a three dimensional measuring system. Anthropol. Sci. 105 (4): 217-229.

Malladi, R. & J. A. Ethian 1996 Image processing: flows under min/max curvature and mean curvature. Graph. Models Image Process. 58 (2): 127-141.

Matsumura, H., M. Nakatsukasa & H. Ishida 1992 Comparative study of crown cusp areas in the dentition of african apes. Bull. Natn. Sci. Mus. Ser. D 18: 1-15.

Ohtake, Y., A. G.Belyaev & I. A. Bogaevski 2000 Polyhedral surface smoothing with simultaneous mesh regularization. Proc. Geometric Modeling and Process. 2000: 229-237.

Spoor, C. F., F. W. Zonneveld & G. A. Macho 1993 Linear measurements of cortical bone and dental enamel by computed tomography: applications and problems. Am. J. Phys. Anthropol. 91: 469-484.

Taubin, G. 1995 A signal processing approach to fair surface design. Siggraph '95: 351-358.

Ungar, P. S. & M. Williamson 2000 Exploring the effects of tooth wear on functional morphology: a preliminary study using dental topographic analysis. Palaeontologia Electronica 3:1. http://palaeo-electronica.org/2000_1/gorilla/main.htm.

Ungar, P. S. 2004 Dental topography and diets of Australopithecus afarensis and early Homo. J. Hum. Evol. 46:605-622.

Wood, B. A. & S. A. Abbott 1983 Analysis of the dental morphology of Plio-Pleistocene hominids. I. Mandibular molars: crown area measurements and morphological traits. J. Anat. 136: 197–219.

Wood, B. A., S. A. Abbott & S. H. Graham 1983 Analysis of the dental morphology of Plio-Pleistocene hominids. II. Mandibular molars – study of cusp areas, fissure pattern and cross sectional shape of the crown. J. Anat. 137: 287–314.

Wood, B. A. & C. A. Engleman 1988 Analysis of the dental morphology of Plio-Pleistocene hominids. V. Maxillary postcanine tooth morphology. J. Anat. 161:1–35.

Zuccotti, L. F., M. D. Williamson, W. F. Limp & P. S. Ungar 1998 Modeling primate occlusal morphology in three dimensions using Geographic Resources Analysis Support System software. (abstract). Am. J. Phys. Anthropol. Suppl. 26: 238-239.